Expert Systems
The Journal of Knowledge Engineering

Article

DOI: 10.1111/j.1468-0394.2010.00525.x

Fuzzy adaptive anisotropic filter for medical images

Recep Demirci
Duzce University, Technical Education Faculty, Electrical Education Department, Konuralp Kampusu, 81620 Duzce, Turkey
Email: recepdemirci@duzce.edu.tr

Abstract: *An adaptive anisotropic diffusion filter for images is proposed in this paper. First, the gradient of an image was calculated by a novel fuzzy-rule-based gradient operator. Accordingly, the centre of gravity of a histogram of the gradient image was estimated and it was assigned as an edge threshold. In conventional anisotropic filters, the conduction coefficients have to be selected by an operator. However, in this study, the centre of gravity of the histogram was assigned as the conduction coefficient of the anisotropic filter. Consequently, an adaptive anisotropic image filter which automatically sets its conduction coefficient without user intervention was developed. The image filter achieved was tested with various medical images.*

Keywords: edge detection, adaptive anisotropic filter, conduction coefficient, medical image

1. Introduction

Processing of medical images has recently become an important tool for clinicians to diagnose diseases. Generally, automated recognition and diagnosis based on medical images involve enhancement, segmentation and quantification tools. Thus the primary step in medical image processing is an enhancement operation which is used to reduce noise and increase the contrast of the structure of interest since medical images are often degraded by noise due to various sources of interference and other phenomena that affect the measurement processes in imaging and data acquisition systems. Fundamentally, image enhancement is the transformation or mapping of one image to another so that desired image features become easier to perceive for the human visual system or more probably detected by automated image analysis systems. Image filtering algorithms were initially based on the concept of Gaussian kernels. Nonlinear filtering techniques which preserve edge features have been proposed by Perona and Malik (1990). As a result anisotropic diffusion image filters have become popular in the medical image processing area. Nevertheless the performance of this type of filter depends on the parameters adjusted by users (Alper *et al.*, 2004; Wong & Chung, 2004). In other words, it is an operator-dependent image filter. Therefore the performance of the denoising operation is closely related to operator experience (Sun *et al.*, 2004; Ghita *et al.*, 2005; Kim *et al.*, 2005). Catte *et al.* (1992) observed some problems with the original functions of the Perona and Malik filter. Several authors have suggested variations or enhancements of these original functions. For example, diffusivity functions suggested by Charbonnier *et al.* (1994) and Weickert *et al.* (1998) are based on the gradient of the image whereas Black *et al.* (1998) proposed an edge stopping function based on robust statistics called Tukey's biweight. Monteil and Beghdadi

(1999) observed an undesirable effect called the 'pinhole effect' of the original diffusion functions and proposed a different version of the diffusion function. Lu *et al.* (2005) have used the standard proportional–integral–derivative (PID) control strategy to minimize the mean square error of the filtered images. Fernandez and Lopez (2006) introduced an anisotropic diffusion filter for speckle by means of statistics of noise and signal. The basic proposal for anisotropic diffusion with fuzzy logic was introduced by Aja *et al.* (2001) where absolute differences between the central pixel and its neighbour in the diffusion direction were used as antecedent and the diffusion coefficient was used as the consequent in a fuzzy reasoning system (Aja *et al.*, 2001). However, the performance of the filter was still dependent on the rules selected. Recently, the fuzzy filter proposed by Aja *et al.* was improved by Song and Tizhoosh (2006) by using wavelet and noise estimators. Nevertheless it has computation complexity and user dependence. In this study, a novel algorithm, which adaptively selects the parameters of the anisotropic diffusion filter without user intervention, has been proposed and tested with medical images.

2. Anisotropic diffusion

Scale-space theory introduced by Witkin (1983) is a framework for multi-scale signal representation developed by the computer vision, image processing and signal processing communities. It is a formal theory for handling image structures at different scales in such a way that fine-scale features can be successively suppressed and a scale parameter t can be associated with each level in the scale-space representation. The basic idea is to embed the original signal into a one-parameter family of gradually smoothed signals, in which the fine-scale details are successively suppressed (Lindeberg, 1990).

Although the idea of scale space is general and applies in arbitrary dimensions, it was generally used for two-dimensional images. In scale-space filtering, for a given image $I_0(x, y)$, its linear scale-space representation is a family of derived signals $I(x, y, t)$ defined by convolution of $I_0(x, y)$ with the Gaussian kernel

$$G(x, y, t) = \frac{1}{2\pi t} \exp\left[\frac{-(x^2 + y^2)}{2t}\right] \tag{1}$$

such that

$$I(x, y, t) = G(x, y, t) * I_0(x, y) \tag{2}$$

where $t = \sigma^2$ is the variance of the Gaussian. Following the scale-space filtering concept, it was shown by Koenderink (1984) that the convolution of $I_0(x, y)$ with the Gaussian kernel is equivalent to the solution of the diffusion equation in two dimensions where the conduction coefficient is constant. Accordingly, the one-parameter family of derived images was viewed as equivalent to the solution of the linear heat conduction or diffusion equation as follows:

$$\frac{\partial I(x, y, t)}{\partial t} = c\nabla^2 I(x, y, t) \tag{3}$$

where c is the diffusion conductance or diffusivity of the equation and ∇^2 is the Laplacian operator. In this case, all locations in the image, including the edges, are smoothed equally. This is, of course, undesirable, and a simple development would be to change c with the location x and y in the image. Thus the linear diffusion equation is converted into a nonlinear diffusion equation with non-homogeneous diffusivity.

In image processing applications, it is desired that smoothing within a region is performed rather than smoothing across the boundaries. This could be achieved by setting the diffusion conductance coefficient to be 1 in the interior of each region and 0 at the boundaries. Accordingly, nonlinear anisotropic diffusion in a two-dimensional medium was proposed by Perona and Malik (1990) as follows:

$$\begin{gathered}\frac{\partial I(x, y, t)}{\partial t} = \operatorname{div}[c(x, y, t)\nabla I(x, y, t)] \\ I(x, y, 0) = I_0(x, y)\end{gathered} \tag{4}$$

where $c(x, y, t)$ is the diffusion conductance or diffusivity of the equation and ∇ is the gradient operator. Consequently blurring took place

separately in each region with no interaction between regions. As a result of this, the boundaries of objects in the image remained sharp. Since the region boundaries or edges are not known in advance, it is required to estimate the location of the edges in the image. Therefore, the selection of a proper function for the diffusion conductance $c(x, y, t)$ is a critical issue. The main approach has been based on the magnitude of the gradient of the image as follows:

$$c(x, y, t) = g(\|\nabla I(x, y, t)\|)$$

where $g(.)$ is called the edge stopping function, which is selected as a decreasing function of the gradient of the image. Hence, it has a maximum value at constant signal regions $g(0) = 1$ where the gradients are zero and falls to zero at the edges where the gradients are large. Perona and Malik proposed two different functions for the conduction coefficient in their initial studies:

$$c(x, y, t) = \exp\left[-(\|\nabla I\|/K)^2\right] \tag{5}$$

and

$$c(x, y, t) = \frac{1}{1 + (\|\nabla I\|/K)^2} \tag{6}$$

where the constant K is selected by the operator. To implement the anisotropic diffusion filter in practice, the partial differential equations must be digitized. A four-nearest-neighbour discretization of equation (4) was proposed by Perona and Malik as

$$I_{i,j}^{t+1} = I_{i,j}^{t} + \lambda[c_N d_N + c_S d_S + c_E d_E + c_W d_W]_{i,j}^{t} \tag{7}$$

where $0 \leq \lambda \leq 1/4$ for the numerical scheme to be stable and N, S, E, W are subscripts for north, south, east and west respectively. The symbol d indicates nearest-neighbour differences and c are the conduction coefficients in each diffusion direction.

3. Gradient of image based on fuzzy logic

In the proposed filter strategy, first the gradient of the image was computed by means of a fuzzy mask which is similar to the Prewitt and Sobel

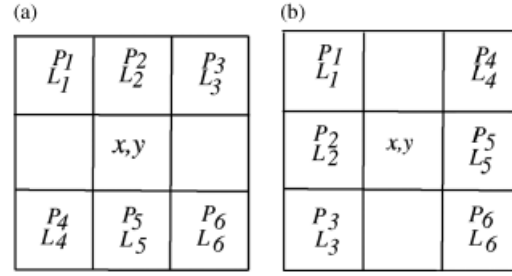

Figure 1: *Fuzzy mask: (a) G_x; (b) G_y.*

mask. Thus two fuzzy masks were employed. The mask in Figure 1(a) was considered for the gradient in the x direction, G_x, while Figure 1(b) was used for the gradient in the y direction, G_y. We define two types of membership functions for the grey level of pixels P_1, P_2, P_3, P_4, P_5 and P_6, as shown in Figures 2(a) and 2(b) where the grey levels have been partitioned by three linguistic values, dark DR, grey GR and white WH. Triangular and Gaussian functions were used. In the membership functions shown in Figure 2(b), overlapping could be controlled by changing the spread of the Gaussian function. In the same way, the membership functions for the derivatives in the x and y directions for the pixel were also defined, as shown in Figures 3(a) and 3(b) respectively. Thirteen linguistic values for the derivative in each direction have been assigned, starting with D_{-6} and ending with D_6.

Generally a fuzzy system is a static mapping between its inputs and outputs. For a fuzzy system the mapping of the inputs to the outputs is characterized by a set of *condition–action* rules or, in *modus pones* (if–then) form, 'if *premise* then *consequent*'. Generally, the inputs of the fuzzy system are associated with the premise, and the outputs are associated with the consequences. These if–then rules can be represented in many forms. Multi-input multi-output (MIMO) and multi-input single output (MISO) are some of the standard forms. The MISO form of linguistic rules in our case is

Rule 1: **If** P_1 is Dark **and** P_2 is Dark **and** P_3 is Dark **and** P_4 is Dark **and** P_5 is Dark **and** P_6 is Dark **then** gradient is D_0

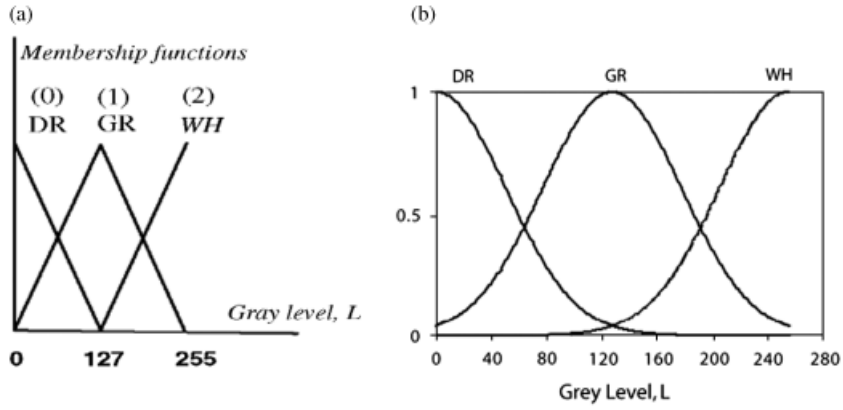

Figure 2: *Membership functions of grey level: (a) triangular; (b) Gaussian.*

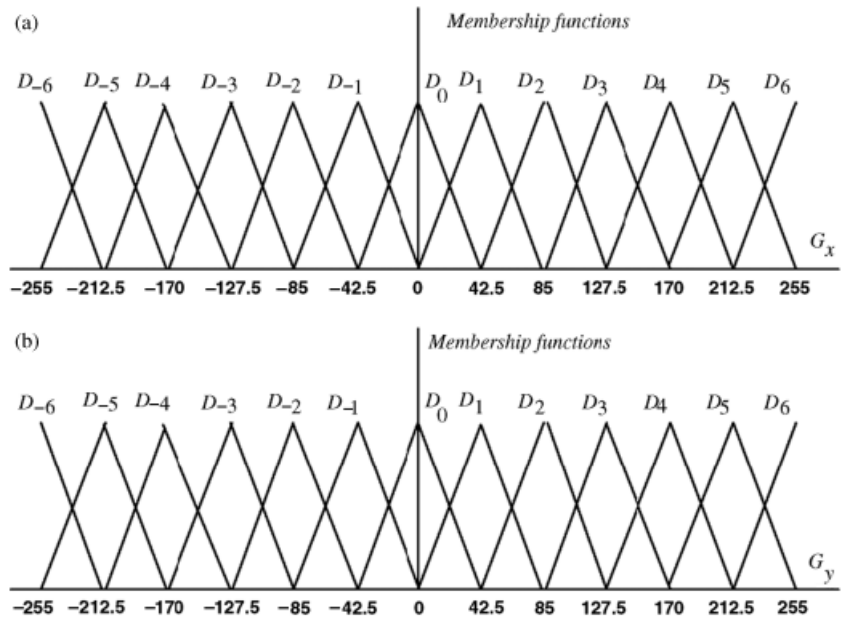

Figure 3: *Membership functions for derivatives in (a) the x direction, G_x; (b) the y direction, G_y.*

Rule 2: **If** P_1 is White **and** P_2 is Dark **and** P_3 is Dark **and** P_4 is Dark **and** P_5 is Dark **and** P_6 is Dark **then** gradient is D_{-2}

and so on.

As a result, rules to compute the gradient of a pixel in the image have been constructed according to Table 1. As there are three linguistic variables, 729 rules in total were established for each derivative. The construction of rules could be done heuristically as shown in Table 1. Nevertheless, in our case an automatic method was used. Each input linguistic variable was indexed with 0 for DR, 1 for GR and 2 for WH, whereas the output linguistic variables were indexed from -6 to 6. For each rule, an index of the membership function for the derivative was found as

$$i = (n + p + r) - (k + l + m) \tag{8}$$

Table 1: *Fuzzy rule table for G_x*

μ_6	μ_5	μ_4	μ_3	μ_2	μ_1	μ_x
DR	DR	DR	DR	DR	DR	D_0
DR	DR	DR	DR	DR	GR	D_{-1}
DR	DR	DR	DR	DR	WH	D_{-2}
DR	DR	DR	DR	GR	DR	D_{-1}
DR	DR	DR	DR	GR	GR	D_{-2}
DR	DR	DR	DR	GR	WH	D_0
.	.	.	.	.	.	
.	.	.	.	.	.	
.	.	.	.	.	.	
WH	WH	WH	WH	WH	WH	D_0

Table 2: *Index table for G_x*

$\mu_6\,(n)$	$\mu_5\,(p)$	$\mu_4\,(r)$	$\mu_3\,(k)$	$\mu_2\,(l)$	$\mu_1\,(m)$	D_i
0	0	0	0	0	0	0
0	0	0	0	0	1	−1
0	0	0	0	0	2	−2
0	0	0	0	1	0	−1
0	0	0	0	1	1	−2
0	0	0	0	1	2	−3
.	.	.	.	.	.	
.	.	.	.	.	.	
.	.	.	.	.	.	
2	2	2	2	2	2	0

where n, p, r, k, l and m are the index numbers of the linguistic variable of each pixel as shown in Table 2. The partial derivatives in both directions were approximated in the same way. When the centriod for defuzzification and the product to represent the conjunctions in the premise are used, then the gradient of pixel (x, y) in the x direction can be explicitly represented as

$$G_x = \frac{\sum_{j=1}^{R} G_j \mu^j_{\text{prem}}(L)}{\sum_{j=1}^{R} \mu^j_{\text{prem}}(L)} \tag{9}$$

where R is the total number of rules for the x direction and $\mu^j_{\text{prem}}(L)$ is the certainty of the premise of the jth rule for the gradient. G_j is the centre of the gradient membership function for the jth rule for the x direction. Furthermore the certainty of the premise of the jth rule for the gradient can be stated as follows:

$$\mu^j_{\text{prem}}(L) = \mu^j_1(L_1)\mu^j_2(L_2)\mu^j_3(L_3)\mu^j_4 \times (L_4) \times \mu^j_5(L_5)\mu^j_6(L_6) \tag{10}$$

4. Automatic edge detection and adaptive diffusion filter

The edge in an image is the deviation of colour intensities from pixel to pixel. Therefore the gradient of the image is required. Once the gradient of the image is calculated, the edges in the image can generally be detected by thresholding the gradient image. In other words, pixels in the image can be clustered into two categories: edge and non-edge. At this stage, a thresholding selection problem occurs. Fortunately, it is observed in the histogram of the gradient image that pixels with small grey level derivations accumulate on the left and pixels with large grey level derivations take place on the right. Therefore in this study an automatic threshold selection method based on the centre of gravity of the histogram is proposed as follows:

$$K = \frac{1}{MN} \sum_{r=0}^{L} r z_r \tag{11}$$

where r is the discrete image intensity level and z_r is the number of pixels with grey level r. M and N denote dimensions of the image and L is the number of distinct intensity levels. Consequently the threshold level K in the output image, which is used to classify pixels as edge and non-edge, is obtained. The well-known camera-man image shown in Figure 4(a) was tested with the proposed algorithm. The gradient of the camera-man image was obtained by means of the fuzzy gradient algorithm with triangular membership functions as shown in Figure 4(b). Then the centre of gravity of the histogram shown in Figure 5(a) was calculated as 11. Accordingly by using this value as an edge threshold, the binary image shown Figure 4(c) was obtained. As can be seen, the edges match very well with human perception.

Then, the gradient of the camera-man image was obtained by means of the fuzzy gradient

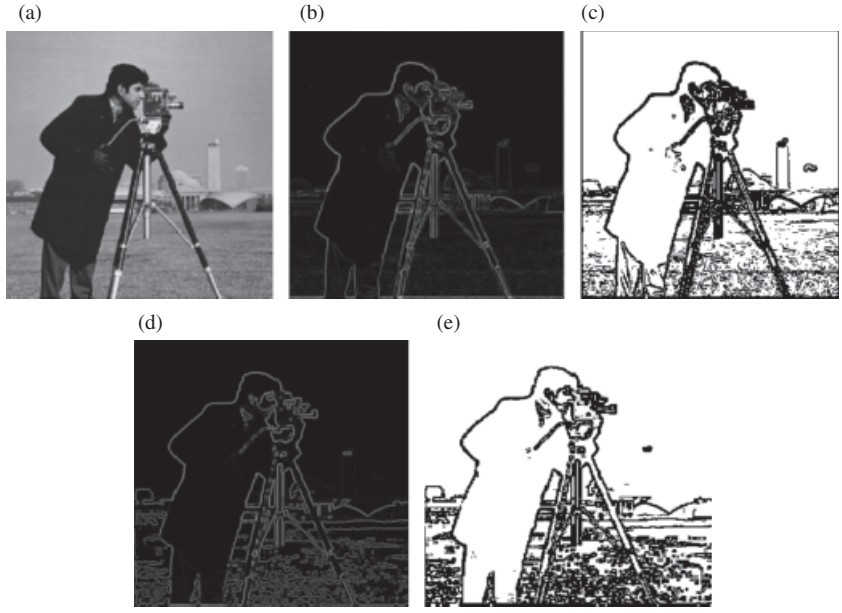

Figure 4: *Camera-man image (a) original; (b) gradient with triangular membership functions; (c) edges with triangular membership functions; (d) gradient with Gaussian membership functions; (e) edges with Gaussian membership functions.*

algorithm with Gaussian membership functions, as shown in Figure 4(d) where the spread of the Gaussian function was set to be 100. Also edges obtained with the Gaussian function are shown in Figure 4(e). Generally, it was observed that a large spread results in small variations being missed in the image. Nevertheless it gives us flexibility to detect different variations by properly selecting the spread.

In image processing applications, it is desired to design a filter which combines low pass filtering in homogeneous regions and a sharpening effect in transition regions. However, it is not easy to design a linear filter which achieves these two conflicting goals. This is why a nonlinear anisotropic diffusion filter has been proposed by researchers. However, there is always a problem to select a proper conductivity function and conduction coefficient. The main philosophy behind the conduction coefficient is that, if a pixel has a small derivation ($d > K$), it must be considered to be in a region and so it must be smoothed more. On the other hand, if a pixel has a large derivation ($d < K$), it must be considered to be an edge and so it must be less smoothed. Consequently, during the filtering process, object boundaries are preserved whereas pixels belonging to objects are smoothed.

To justify our proposal, conductivity functions and a normalized histogram of the gradient of the image were plotted on the same chart, as shown in Figure 5(b). Three well-known conductivity functions, the Perona and Malik, the Charbonnier and the Weickert, have been considered. The meaning of the chart is that pixels lower than K will be more smoothed because they belong to regions. However, pixels larger than K will be less smoothed as they belong to edges.

5. Simulation results and discussion

To evaluate the efficiency of the proposed approach, original images corrupted by Gaussian white noise and speckle noise are considered.

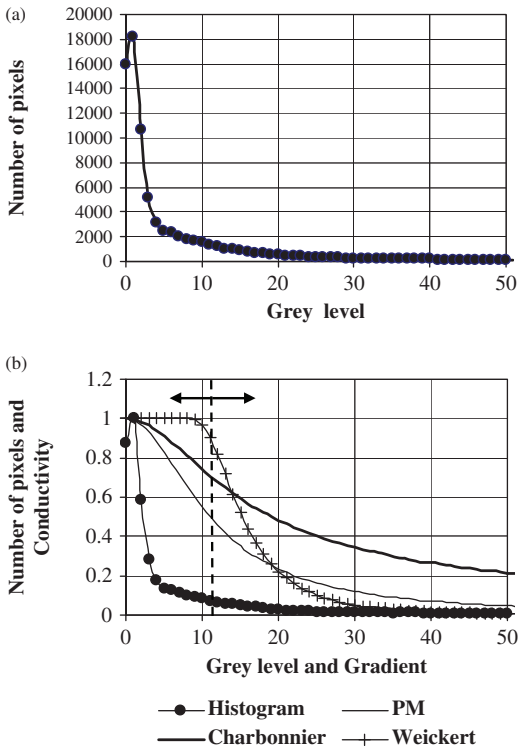

Figure 5: *(a) Histogram of the gradient of the camera-man with triangular membership functions; (b) normalized histogram and different conductivity functions. (PM, the Perona and Malik function.)*

For subjective comparison only, visual judgement is used, while for objective comparison the mean square error (MSE) is used. The MSE is given by

$$\mathrm{MSE} = \frac{1}{MN}\sum_{i=0}^{M-1}\sum_{j=0}^{N-1}\left[I_0(x_i, y_j) - I_\mathrm{f}(x_i, y_j)\right]^2 \tag{12}$$

where I_0 and I_f are the original and the filtered images, respectively. Moreover M and N are the dimensions of the images. Also the noise value of the corrupted image was calculated from the peak signal-to-noise ratio (PSNR) as follows:

$$\mathrm{PSNR} = 10\log\left(\frac{255 \times 255}{\mathrm{MSE}}\right) \tag{13}$$

The proposed algorithm was tested with a CT image shown in Figure 6(a) which has a size of 274×232 with 255 grey levels. The gradient of the image computed by the fuzzy mask is shown in Figure 6(b) while the edges obtained with automatic thresholding are shown in Figure 6(c). The image contaminated with Gaussian noise shown in Figure 6(d) was filtered with different edge stopping methods. Figure 6(e) shows the performance of the adaptive anisotropic diffusion filter of Perona and Malik while the results with the Charbonnier filter are shown in Figure 6(f). Moreover the output of the adaptive diffusion filter with the Weickert function is shown in Figure 6(g).

The performance of the proposed filter with different edge stopping functions was also tested for the CT image shown in Figure 7(a) where speckle noise was added. The results with the Perona and Malik, Charbonnier and Weickert functions are shown in Figures 7(b), 7(c) and 7(d), respectively. As can be seen, the MSE with the three functions is quite low.

The developed diffusion filter was also tested for colour images. The stages explained above were applied for every colour component separately. Consequently, different diffusion conduction coefficients for each component were computed automatically. However, only red components of the images were considered when calculating the performance measure of the filter with equations (12) and (13). Therefore, the MSE and PSNR given for colour images are only for the red components. Figure 8(a) shows a tissue image of an intestine biopsy which is commonly used to diagnose cancer. Artificial Gaussian noise was added to the original, as shown in Figure 8(b). The filtered biopsy image with the Perona and Malik function is shown in Figure 8(c) whereas Figure 8(d) shows the filter performance with the Charbonnier function. In addition, the contaminated biopsy image was filtered using the Weickert function, as shown in Figure 8(e).

Additionally, the tissue image of an intestine biopsy was degraded with speckle noise as shown in Figure 9(a) and then filtered with the edge stopping functions used in the previous

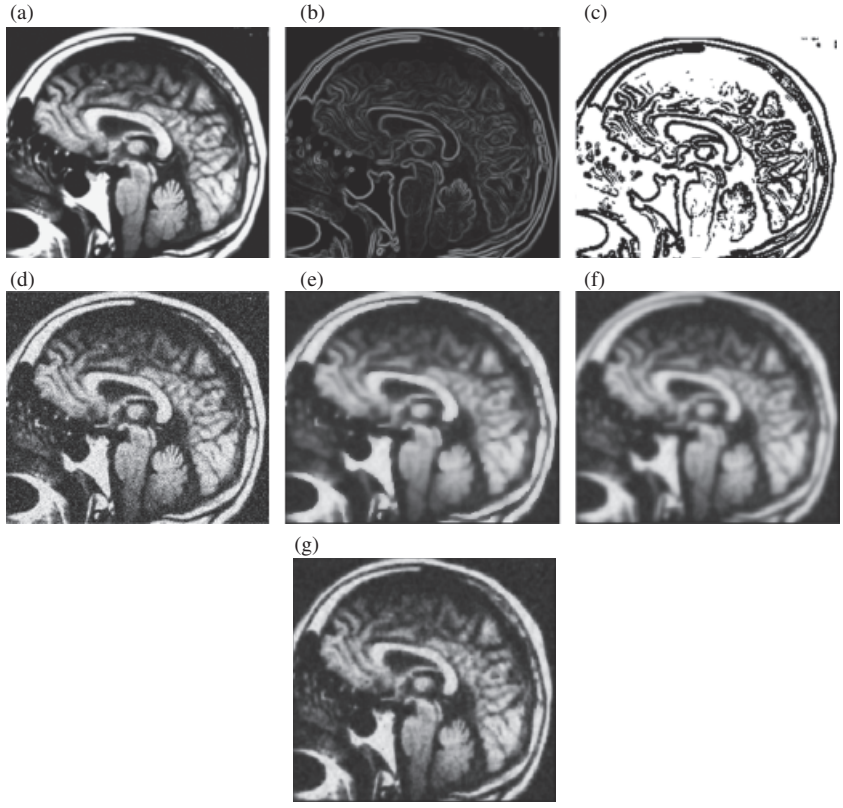

Figure 6: *CT image: (a) original; (b) gradient with fuzzy (c) edge (d) contaminated with Gaussian noise (PSNR = 18 dB); (e) denoised with the Perona and Malik function (t = 20, MSE = 0.526); (f) denoised with the Charbonnier function (t = 20, MSE = 0.580); (g) denoised with the Weickert function (t = 20, MSE = 0.479).*

experiments. As was done for the previous examples, the conductance parameters were calculated with equation (11) and then used within filtering operations. The resulting denoised images with the Perona and Malik, Charbonnier and Weickert functions are shown in Figures 9(b), 9(c) and 9(d), respectively.

It was noticed from applications that the grey scale or medical colour images are successfully filtered without requiring any pre-knowledge from the operator. Furthermore, the above results were obtained with only 20 iterations. On the other hand, in the conventional diffusion filter approach, if the conductivity parameter is chosen to be larger, the edge preserving feature of the diffusion filter may be lost. If the conductivity is selected to be small, more iterations are required to achieve a good noise reduction performance. Consequently, the proposed algorithm can automatically not only find edges but also set the diffusion conductance. So there will be no need for the clinician to enter parameters during the denoising operation.

6. Conclusion

A novel adaptive anisotropic diffusion filter for medical images was developed. With the proposed image filter, operator dependence was avoided. Moreover, a new approach to calculate the gradient of two-dimensional images by

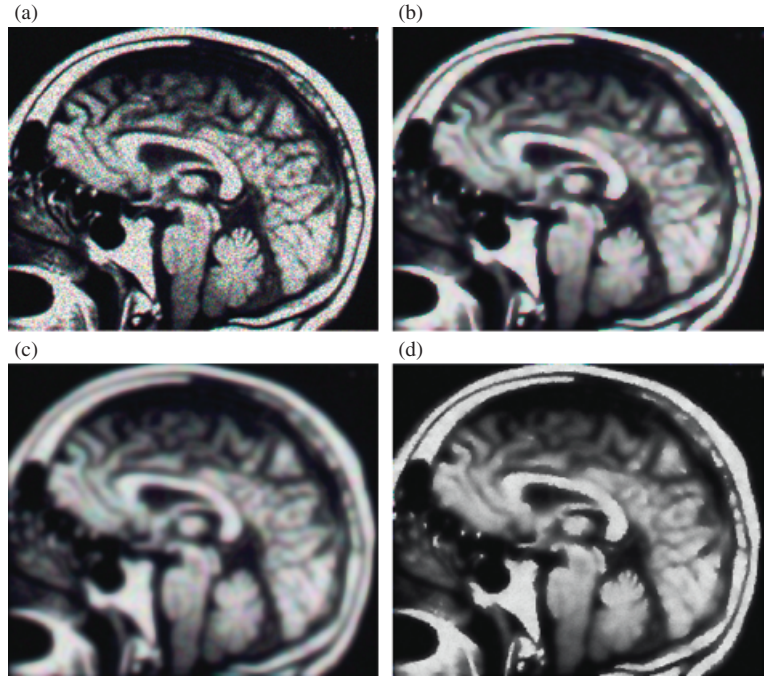

Figure 7: *(a) CT image contaminated with speckle noise (PSNR = 18 dB); (b) denoised with the Perona and Malik function (t = 20, MSE = 0.520); (c) denoised with the Charbonnier function (t = 20, MSE = 0.617); (d) denoised with the Weickert function (t = 20, MSE = 0.819).*

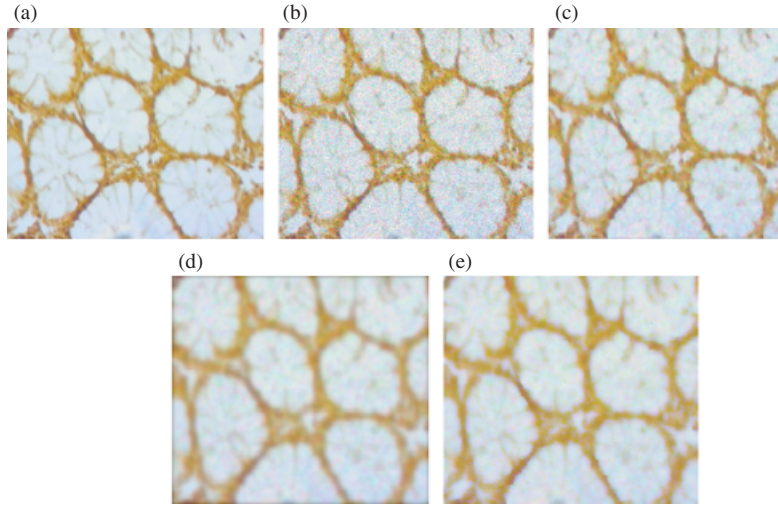

Figure 8: *A tissue image of an intestine biopsy: (a) original; (b) contaminated with Gaussian noise (PSNR = 22 dB); (c) denoised with the Perona and Malik function (t = 20, MSE = 0.417); (d) denoised with the Charbonnier function (t = 20, MSE = 0.827); (e) denoised with the Weickert function (t = 20, MSE = 0.714).*

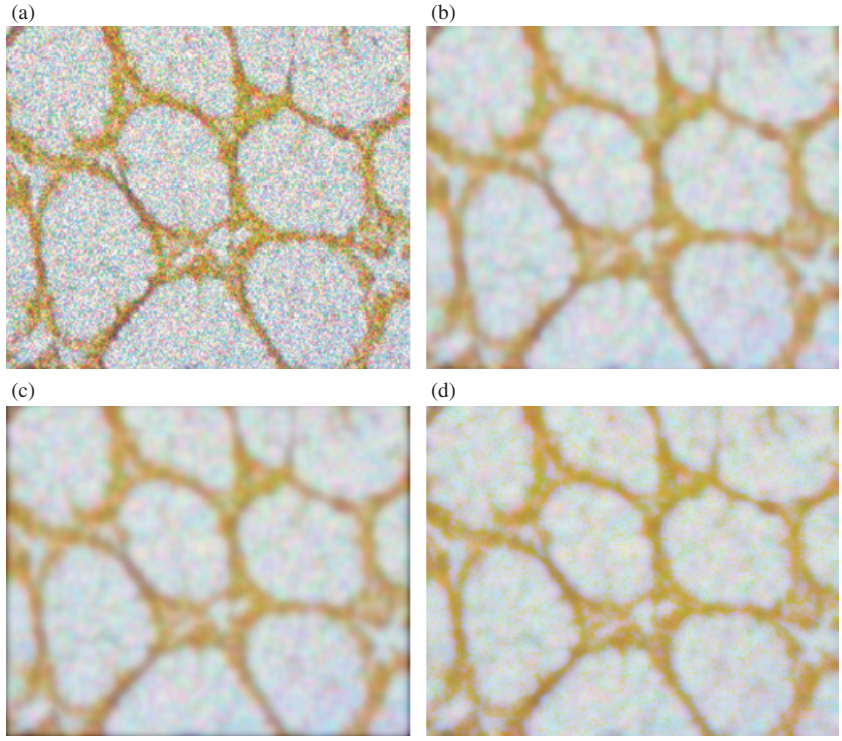

Figure 9: *(a) A tissue image of an intestine biopsy contaminated with speckle noise (PSNR = 16 dB); (b) denoised with the Perona and Malik function (t = 20, MSE = 0.567); (c) denoised with the Charbonnier function (t = 20, MSE = 0.226); (d) denoised with the Weickert function (t = 20, MSE = 0.693).*

means of fuzzy reasoning rules was proposed. This gives us the flexibility to implement image processing algorithms in fuzzy processor chips. Also it was justified that the centre of gravity of the histogram of the gradient image could be used as a threshold for edge detection in image processing. Finally, it was observed that the proposed image filter could be successfully used in medical image processing applications.

References

Aja, S., C. Alborola and J. Ruiz (2001) Fuzzy anisotropic diffusion for speckle filtering, in *IEEE International Conference on Acoustics, Speech, and Signal Processing*, Washington, DC: IEEE Computer Society, Vol. 2, pp. 1262–1264.

Alper, M., A. Kavak, A.H. Parlak, R. Demirci, I. Belenli and N. Yesildal (2004) Measurement of epidermal thickness in a patient with psoriasis by computer-supported image analysis, *Brazilian Journal of Medical and Biological Research*, **37**, 111–117.

Black, M.J., G. Sapiro, D.H. Marimont and D. Heeger (1998) Robust anisotropic diffusion, *IEEE Transactions on Image Processing*, **7** (3), 421–432.

Catte, F., P.L. Lions, J.M. Morel and T. Coll (1992) Image selective smoothing and edge detection by nonlinear diffusion, *SIAM Journal of Numerical Analysis*, **29**, 182–193.

Charbonnier, P., L.B. Feraud, G. Aubert and M. Barlaud (1994) Two deterministic half-quadratic regularization algorithms for computed imaging, in *Proceedings of ICIP-94 IEEE International Conference on Image Processing*, New York: IEEE Press, Vol. 2, pp. 168–172.

Fernandez, S.A. and C.A. Lopez (2006) On the estimation of the coefficient of variation for

anisotropic diffusion speckle filtering, *IEEE Transactions on Image Processing*, **15** (9), 2694–2701.

GHITA, O., K. ROBINSON, M. LYNCH and P.F. WHELAN (2005) MRI diffusion-based filtering: a note on performance characterization, *Computerized Medical Imaging and Graphics*, **29** (4), 267–277.

KIM, H.Y., J. GIACOMANTONE and Z.H. CHO (2005) Robust anisotropic diffusion to produce enhanced statistical parametric map from noisy fMRI, *Computer Vision and Image Understanding*, **99** (3), 435–452.

KOENDERINK, J. (1984) The structure of images, *Biological Cybernetics*, **50**, 363–370.

LINDEBERG, T. (1990) Scale-space for discrete signals, *IEEE Transactions on Pattern Analysis and Machine Intelligence*, **12** (3), 234–254.

LU, R., Y. SHEN and Y. WANG (2005) Novel anisotropic diffusion algorithm based on PID control law together with stopping mechanism, in *IEEE-EMBS 2005, 27th Annual International Conference on Engineering in Medicine and Biology*, New York: IEEE Press, 3402–3405.

MONTEIL, J. and A. BEGHDADI (1999) A new interpretation and improvement of the nonlinear anisotropic diffusion for image enhancement, *IEEE Transactions on Pattern Analysis and Machine Intelligence*, **21** (9), 940–946.

PERONA, P. and J. MALIK (1990) Scale-space and edge detection using anisotropic diffusion, *IEEE Transactions on Pattern Analysis and Machine Intelligence*, **12** (7), 629–939.

SONG, J. and H.R. TIZHOOSH (2006) Fuzzy anisotropic diffusion based on edge detection, *Journal of Intelligent and Fuzzy Systems*, **17** (5), 431–442.

SUN, O., J.A. HOSSACK, J. TANG and S.T. ACTON (2004) Speckle reducing anisotropic diffusion for 3D ultrasound images, *Computerized Medical Imaging and Graphics*, **28** (8), 461–470.

WEICKERT, J., B.M. TER H. ROMENY and M. VIERGEVER (1998) Efficient and reliable schemes for nonlinear diffusion filtering, *IEEE Transactions on Image Processing*, **7** (3), 398–410.

WITKIN, A. (1983) Scale space filtering, in *Proceedings of the 8th International Joint Conference on Artificial Intelligence*, A. Bundy (ed.), Los Altos, CA: William Kaufmann, Vol. 2, pp. 1019–1022.

WONG, W.C.K. and A.C.S. CHUNG (2004) A nonlinear and non-iterative noise reduction technique for medical images: concept and methods comparison, in *International Congress Series 1268*, Amsterdam, Elsevier, 171–176.

The author

Recep Demirci

Recep Demirci studied electrical education at Gazi University and received a BSc degree in 1990. He was a visiting researcher at Purdue University, USA, in 1992, and he received a PhD degree from the Electrical Engineering Department, University of Wales, Cardiff, UK, in 1998. He worked as an assistant professor at the Electrical Education Department, Technical Education Faculty, Abant Izzet Baysal University, from 2000 to 2006, and he has been working as an assistant professor at the Electrical Education Department, Technical Education Faculty, Duzce University, since 2006.